Chemosphere 358 (2024) 142222

Contents lists available at ScienceDirect

Chemosphere

journal homepage: www.elsevier.com/locate/chemosphere

Unveiling the potential of machine learning in cost-effective degradation of pharmaceutically active compounds: A stirred photo-reactor study

B. Acosta-Angulo [a], J. Lara-Ramos [a], A. Niño-Vargas [a], J. Diaz-Angulo [b], J. Benavides-Guerrero [c], A. Bhattacharya [c], S. Cloutier [c], F. Machuca-Martínez [a,*]

[a] Escuela de Ingeniería Química, Universidad Del Valle, Santiago de, Cali, 760026, Valle Del Cauca, Colombia
[b] Research and Technological Development in Water Treatment, Processes Modelling and Disposal of Residues – GITAM, Cauca, Colombia
[c] Department of Electrical Engineering, Ecole de Technologia Superieure, 1100 Notre-Dame West, Montreal, H3C 1K3, Quebec, Canada

HIGHLIGHTS

- Machine Learning to predict degradation kinetics of water pollutants.
- Cost-efficiency optimization over the PhACs degradation through intensified AOPs.
- Artificial neural networks allow correlation between descriptors and degradation of pollutants.
- Ozone-based processes offered the fastest kinetics for the removal of the evaluated contaminants.

GRAPHICAL ABSTRACT

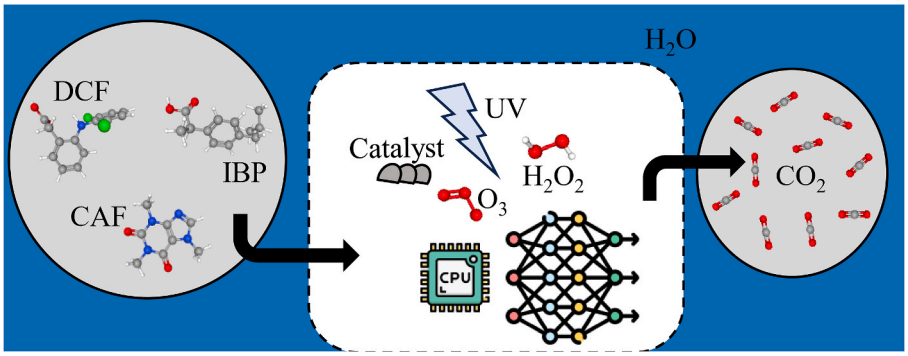

ARTICLE INFO

Handling editor, Kaan Yetilmezsoy

ABSTRACT

In this study, neural networks and support vector regression (SVR) were employed to predict the degradation over three pharmaceutically active compounds (PhACs): Ibuprofen (IBP), diclofenac (DCF), and caffeine (CAF) within a stirred reactor featuring a flotation cell with two non-concentric ultraviolet lamps. A total of 438 datapoints were collected from published works and distributed into 70% training and 30% test datasets while cross-validation was utilized to assess the training reliability. The models incorporated 15 input variables concerning reaction kinetics, molecular properties, hydrodynamic information, presence of radiation, and catalytic properties. It was observed that the Support Vector Regression (SVR) presented a poor performance as the ε hyperparameter ignored large error over low concentration levels. Meanwhile, the Artificial Neural Networks (ANN) model was able to provide rough estimations on the expected degradation of the pollutants without requiring information regarding reaction rate constants. The multi-objective optimization analysis suggested a leading role due to ozone kinetic for a rapid degradation of the contaminants and most of the results required intensification with hydrogen peroxide and Fenton process. Although both models were affected by accuracy limitations, this work provided a lightweight model to evaluate different Advanced Oxidation Processes (AOPs)

* Corresponding author.
E-mail address: fiderman.machuca@correounivalle.edu.co (F. Machuca-Martínez).

https://doi.org/10.1016/j.chemosphere.2024.142222
Received 7 November 2023; Received in revised form 30 March 2024; Accepted 30 April 2024
Available online 5 May 2024

by providing general information regarding the process operational conditions as well as know molecular and catalytic properties.

1. Introduction

Contaminants of emerging concern (CECs), particularly pharmaceutically active compounds (PhACs) have gathered significant concern due to their potential impact on aquatic ecosystems and human health upon prolonged exposure (Ben Chabchoubi et al., 2023; Christou et al., 2017). Over the last decade, the release of unmetabolized antibiotics into the environment has been shown to contribute to the development of antibiotic-resistant bacteria (Majumder et al., 2021). This situation exposes the need to improve the management of pharmaceutical residues in water systems. As such, further development is required on industrial wastewater treatment plants (WWTPs) as there is strong evidence supporting inefficient removals over an extensive list of CECs (Svebrant et al., 2021).

In this regard, the Advanced Oxidation Processes (AOPs) have been widely investigated as effective alternatives for water decontamination proving to yield high rates of removal for different types of CECs (Feijoo et al., 2023; Kumar et al., 2023; Rodríguez-Chueca et al., 2023). Although the efficiency of AOPs is limited by factors concerning the transport phenomena, production of hazardous by-products, and energy consumption (Lian et al., 2022; Constantino et al., 2022; Ji et al., 2022), the intensification of AOPs through the integration of several processes has become a highly attractive approach as it has been proved to overcome some of the limitations from the conventional AOPs owing to synergistic effects triggered by the interaction with catalysts and additional reagents (Fischbacher et al., 2013; Sirés et al., 2014; Babuponnusami and Muthukumar, 2014; Lara-Ramos et al., 2019).

Nevertheless, there is still a gap in the efficient scaling of these systems into large operational contexts, where design challenges arise due to transport phenomena limitations and the costs linked to the technologies (Méndez-Arriaga et al., 2009). Therefore, the AOPs degradation kinetics remains an active research topic. This field has been mostly explored through experimentation, but also, phenomenological mathematical models have been implemented to gain additional insight into the reaction kinetics (Tong et al., 2020; Acosta-Angulo et al., 2021; Ding and Hu, 2021). This approach turns out particularly important to study variables that cannot be easily measured, as is the case for the volumetric rate of photon absorption (LVRA) within heterogeneous photocatalytic reactors (Acosta-Herazo et al., 2020), its corresponding evolution due to photo-sensitization (Diaz-Angulo et al., 2019), the mass transfer interactions between multiple phases (Li et al., 2021), the flow mixing over different reactor geometries (Pathapati et al., 2016), among other variables (He et al., 2023; Xiao et al., 2017).

Although phenomenological mathematical models are powerful tools, as they rely upon the physicochemical governing principles of the processes, their accuracy is strongly dependent on the complexity and number of important effects required to model the system of interest. Thus, in the case of reactive systems involving the influence of multiple species, the model complexity increases considerably and quantum mechanics approaches such as Density Functional Theory (DFT) and molecular simulation are often required (Ngo et al., 2023; Shahsavar et al., 2023), which demands high computational costs.

Accordingly, this research has delved into an alternative exploration of AOPs kinetics through Machine Learning (ML) to provide a lightweight tool to approximately predict the degradation performance for different AOPs. Such an approach has been motivated by the high impact of ML-based models in several fields, including the study of reaction kinetics (Gbadago et al., 2021; Murakami and Shono, 2022; Zhu et al., 2023). These kinds of models rely on features that are expected to exhibit a strong correlation with the response variables. Although they cannot directly provide a phenomenological explanation, these models can leverage the availability of information to explain variance in the response variables due to the input features which is done through training algorithms concerning supervised, unsupervised, semi-supervised, and reinforcement strategies (Cherian Joel Mathewand Kumar et al., 2023).

Once a Machine-Learning model has been trained, it can compute outputs in significantly shorter periods compared to robust state-of-the-art phenomenological models. This makes ML particularly attractive for industrial and control applications, where the rapid prediction of variables is desired to monitor and optimize aspects such as the yield and selectivity for chemical reactions, the amount of released heat in exothermic processes, or the products manufacturing quality related to *in situ* measurable variables, as temperature, pressure, concentration of reagents, flow rates or densities (Gao et al., 2022).

1.1. Machine learning in AOPs

From a general perspective, the popularity of machine learning implementations has rapidly increased in several disciplines due to their potential for recognizing complex patterns (Telikani et al., 2021). Historically, artificial neural networks (ANN) have been the predominant machine learning-based technique in AOPs research. However, accelerated growth has been observed for alternative approaches since 2013. Fig. 1 contrasts the number of publications in the AOPs field regarding neural networks against alternative ML approaches according to the search equations: (i) TITLE-ABS-KEY{("neural network*") AND ("advanced oxidation process*" OR "AOP*")}, and (ii) TITLE-ABS-KEY {("machine learning") AND ("advanced oxidation process*" OR "AOP*") AND NOT ("neural network*")}.

In 2019, Mojiri et al. (2019) employed a feed-forward neural network consisting of a single hidden layer with four neurons to predict the degradation of acetaminophen and amoxicillin through ozonation. The trained network was employed to optimize the removal efficiency while varying the initial ozone dosage and pollutant concentration. Even though a simple network architecture was implemented, the model was able to maximize the removal efficiency for the pollutants with an acceptable accuracy.

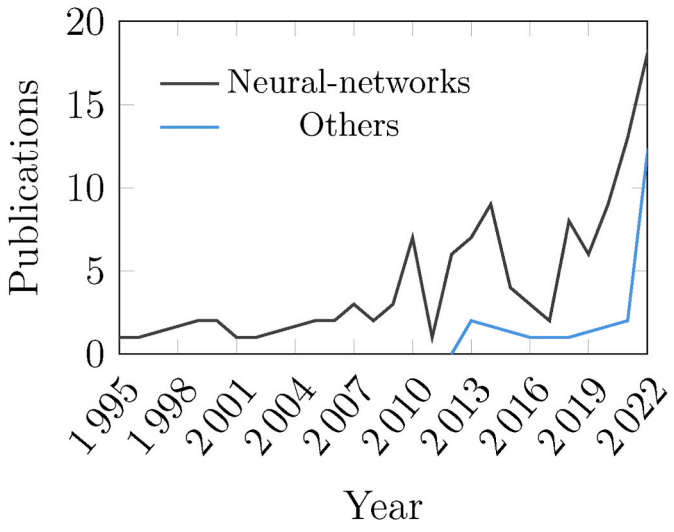

Fig. 1. Publications regarding the use of neural networks and alternative machine learning approaches in the AOPs research retrieved from the Scopus database.

Later, in 2020, a single hidden layer neural network was implemented by Feliciano et al. (Rayssa et al., 2020) to predict the degradation of lamivudine through photo-peroxidation employing the reaction period, hydrogen peroxide dose, and initial pollutant concentration as input features. The hidden layer was comprised of 12 neurons and the available data was distributed into 70, 15, and 15% corresponding to training, test, and validation datasets, respectively. Also, Huang et al. (2020) employed two QSAR models based on multi-linear and support vector regressions (SVR) to predict the ozone reaction rate constants for several pollutants, and their study found that SVR presented the best fitting performance.

A similar approach was implemented by Tangestani et al. (2021) in 2021 to predict reaction rate constants with hydroxyl radicals throughout three ML-models: decision trees (DT), least-squares support vector machine (LSSVM), and adaptive neuro-fuzzy inference system (ANFIS). They found that DT presented the best performance, followed by LSSVM. Then, in 2022, Nasseh et al. (2022) utilized a neural network-based approach to predict the photocatalytic degradation of tamoxifen in a nanocomposite $FeCl_2$/AC/ZnO catalyst, and Liu et al. (2022) implemented a support vector regression model to predict the degradation of diclofenac through digestate-derived catalyzed peroxymonosulfate oxidation.

Despite the recent advances, Machine Learning implementations for AOPs are still in an early stage of implementation and more development is required to model the integrated effect of different AOPs. As such, this work compared the performance of two ML models: SVR and ANN, to predict the degradation of three different PhACs in a flotation cell-based reactor. Thus, accuracy and reliability tests were implemented to assess the most suitable approach for the task, while a mathematical model for the operating costs of the reactor was simultaneously formulated. Then, a multi-objective optimization was performed to identify cost-efficient configurations for the removal of the target pollutants.

These results provide a significant contribution to the AOPs research as to the best of the authors' knowledge it is the first time that a single model allows the evaluation of different AOPs by also considering distinct target contaminants without explicitly requiring values for the reaction rate constants. However, due to accuracy limitations, the model should not be thought of as a generalized predictive tool since it was only trained and validated over stirred batch systems operating in the range of 900–1500 rpm, and treatment volumes from 2 to 4.5 L according to the experimental works from Lara et al. (Lara-Ramos et al., 2019; Lara-ram et al., 2021; Afreen et al., 2021; Lara-Ramos et al., 2021a).

2. Methods

This research was comprised of six stages consisting of (i) collecting data for the degradation of PhACs through different AOPs, (ii) identifying input variables, (iii) ANN and SVR settings, (iv) models sensitivity analysis, (v) the estimation of operating costs, and (vi) the multi-objective optimization. These steps are further explained in Sections 2.1 - 2.6. The procedures regarding neural network architecture and training were performed using the Pytorch package (Adam et al., 2019), and the SVR was supported in the Scikit-learn package (Pedregosa FABIANPEDREGOSA et al., 2011).

2.1. Data collection

The experimental data was retrieved from Lara et al. (Lara-Ramos et al., 2019; Lara-ram et al., 2021; Afreen et al., 2021; Lara-Ramos et al., 2021a) research on the degradation of ibuprofen (IBP), diclofenac (DCF), and caffeine (CAF) through different AOPs. In their works, the UHPLC technique was utilized to track the PhACs degradation. Their experiments were performed in the system shown in Fig. 2. There, three different catalysts were evaluated: TiO_2 Aeroxide p25 (Ti-p25), laboratory-scale synthesized TiO_2 nanowires (Ti-Nw), and catalyst grade Goethite (FeOOH) from Merk.

The experimental setup was comprised of a modified flotation cell with two non-concentric fluorescent tubular lamps (Repti Glo 5.0 compact 20 W), emitting wavelengths between 290 and 690 nm with two maxima at 385 and 540 nm. A storage tank whose volume was evaluated in the range from 2 to 4.5 L, a rotor with angular speed capacity for 300–3300 rpm. The ozone was produced with an A2Z 5glab unit that was fed with industrial-grade oxygen. All the degradation experiments were carried out at ambient temperature and circumneutral pH, while the pressure drop was considered negligible.

the retrieved information corresponded to oxidation processes employing: (i) Photolysis, (ii) heterogeneous photocatalysis, (iii) peroxidation, (iv) heterogeneous Fenton, (v) ozonation, (vi) Fenton/O3, (vii) Peroxone, (viii) catalytic ozonation, and (ix) photocatalytic ozonation. In the current study, each of the collected samples corresponds to a pollutant concentration at a given time $t > 0$.

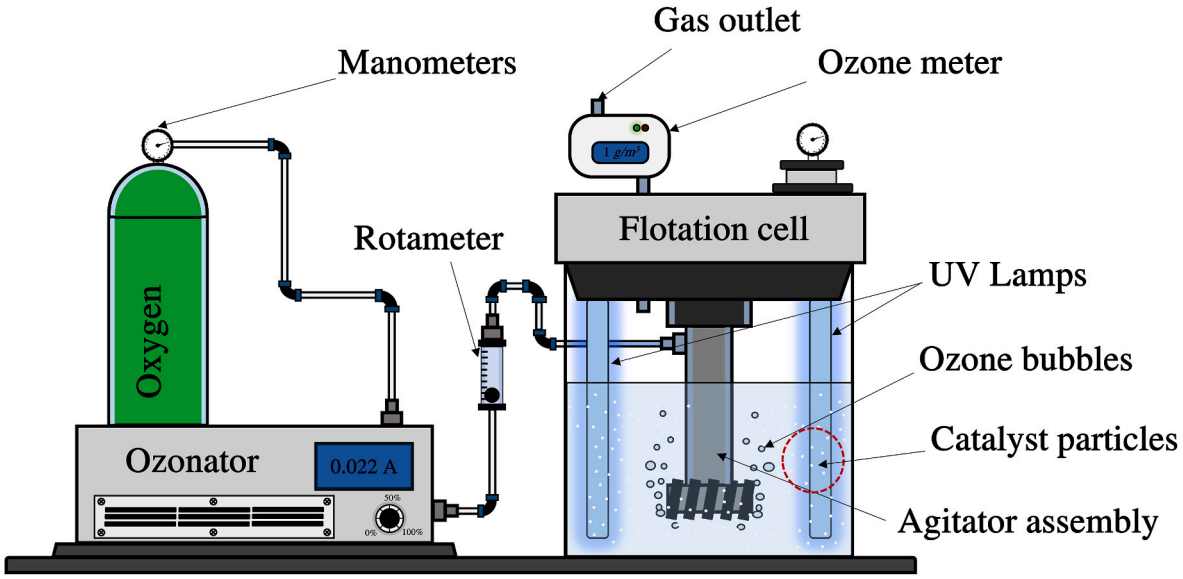

Fig. 2. Experimental setup of the gas-liquid stirred photoreactor, retrieved from (Lara-Ramos et al., 2019).

2.2. Variables normalization

The model input was comprised of 15 descriptors and they were normalized according to the MinMax normalization function (Singh and Singh, 2020). The criteria for selecting the inputs consisted in collecting information that allowed the model to distinguish between different AOPs and target pollutants without the use of categorical variables. Among these inputs, five groups were distinguished regarding kinetic (i), molecular (ii), hydrodynamic (iii), radiation (iv), and catalytic contributions (v). They are further described in Sections 2.2.1 - 2.2.5, where the minimum and maximum values corresponded to the operating ranges for the experimental data.

2.2.1. Kinetic descriptors

The initial concentration for pollutant and oxidizing species, the gas phase ozone mole flow, and the expected reaction time were considered as input variables that carried information regarding the extent of the pollutant degradation. Table 1 provides the ranges for these inputs as well as the normalization parameters (see Table 2).

Accordingly, it was expected that the model established a proportional relationship between the reaction time, the initial concentration, and the expected removal. Meanwhile, the strength of such an effect had to be modified by the ozone and hydrogen peroxide features.

2.2.2. Molecular descriptors

This group was composed of intrinsic properties of the PhACs molecules, namely: the number of hydrogen-bond acceptors (HA), hydrogen-bond donors (HD), molecular polar surface area (PSA), and molecular weights (Mw). These variables were employed to allow the model to distinguish between different PhACs, their ranges are described in Table 3.

These features were selected considering that the molecular weight can work as a classifier for different chemical compounds but, in organic chemistry, two or more molecules can describe the same Mw while exhibiting distinct chemical behaviors (McMurry, 2003). Consequently, additional information was required. In this regard, information regarding the polar properties of the molecules was utilized as an indicator of their affinity to undergo oxidation-reduction reactions. As such, the PSA was employed as a likelihood factor for polar interactions (Prasanna and Doerksen, 2009) while the HA and HD, which are known descriptors in drug design (Coimbra et al., 2020), were considered as potential locations for interactions between the pollutants and the oxidizing species (Choi et al., 2020; Smith, 2021).

2.2.3. Hydrodynamic descriptors

This group included the effect of the reactor volume and the rotor angular speed. It was intended to represent the degree of mixing within the system. The operating ranges and normalization parameters are described in Table 3.

Here, volume was expected to provide an inverse relationship with the extent of the reaction since large systems are more sensitive to transport phenomena limitations. Conversely, the stirring speed contributed to reducing part of these limitations by improving the degree of mixing.

Table 1
Normalization parameters for the kinetic descriptors.

Variables	Min. Value	Max. Value	Mean	σ	Units	Labels
t	2.0	20.0	11.0	5.7	$min min$	x_1^*
c_{PhACs}	15.1	183.9	109.0	42.0	mM	x_2^*
c_{O_3}	0.0	208.3	76.8	57.4		x_3^*
$c_{H_2O_2}$	0.0	470.6	24.0	100.0		x_4^*
F_{O_3}	0.0	416.7	143.4	122.2	$mmol\ min^{-1}$	x_5^*

Table 2
Normalization parameters for the molecular descriptors.

Variables	Min. Value	Max. Value	Mean	σ	Units	Labels
HA	2.00	3.00	2.83	0.37		x_6^*
HD	0.00	2.00	1.16	0.90		x_7^*
PSA	37.30	58.40	50.34	7.15	$Å^2$	x_8^*
Mw	194.14	296.10	296.10	49.10	$mg\ mmol^{-1}$	x_9^*

Table 3
Normalization parameters for the hydrodynamic descriptors.

Variables	Min. Value	Max. Value	Mean	σ	Units	Labels
V	2.0	4.5	2.9	1.1	L	x_{10}^*
ω	900.0	1500.0	1422.5	152.7	rpm	x_{11}^*

2.2.4. Radiation descriptors

Since no information concerning the emission wavelength for the lamps could be obtained, its effect was described through a binary variable whose values corresponded to the absence or presence of irradiation, according to 0 and 1, respectively. Since all the collected experiments were performed under a similar UV-spectrum it was assumed that this simplification would be adequate to describe the photonic effect in the reactor.

2.2.5. Catalytic descriptors

The catalyst load (C_{mp}), specific surface (S_g), and energy band gap (ΔE_g) were selected as the variables representing catalytic effects during the degradation of PhACs. Their ranges and normalization parameters are presented in Table 4.

Since all the collected experiments involving the use of catalysts were carried out in suspension, the inputs C_{mp} and S_g were intended to represent the volumetric availability of active surface (Acosta-Angulo et al., 2021). Meanwhile, the band gap was expected to represent the catalyst photoactivity.

2.3. Models formulation

Two different approaches: ANN and SVR were evaluated to predict the normalized degradation of PhACs in the flotation cell based on the moles of converted pollutant per reaction volume. The training performance was evaluated for two different normalization functions at the output variable, corresponding to the MinMax, Eq. (1), and Z-score regularization, Eq. (2) (Singh and Singh, 2020).

$$y^* = \frac{y - y_{min}}{y_{max} - y_{min}} \tag{1}$$

$$y^* = \frac{y - \overline{y}}{\sigma} \tag{2}$$

Accordingly, data was distributed into 70% training and 30% test. Also, a shuffle-splitting cross-validation technique was employed to assess the models reliability (Yates et al., 2023), the distribution over each iteration is presented in Fig. 3.

Randomly switching elements from the training and test datasets allowed to avoid singular patterns in data that might introduce bias in the model (see Fig. 4). This becomes desirable for validation purposes as

Table 4
Normalization parameters for the catalytic descriptors.

Variables	Min. Value	Max. Value	Mean	σ	Units	Labels
ΔE_g	0.00	3.20	0.57	1.21	eV	x_{13}^*
S_g	0.00	50.00	13.95	20.55	$m^2 g^{-1}$	x_{14}^*
C_{mp}	0.00	1.00	0.32	0.31	$g\ L^{-1}$	x_{15}^*

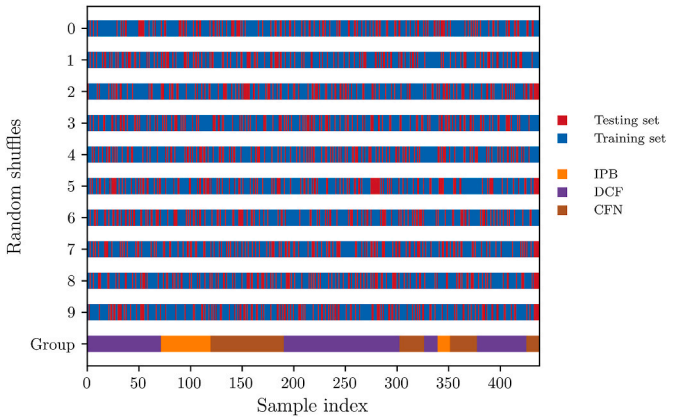

Fig. 3. Distribution for a cross-validation using 10 random shuffles between the training and test datasets.

it is required to demonstrate that the variance contained in any random subset which is large enough to train the model, is a good representation of the global variance. Therefore, random extraction of elements for the training dataset should lead to similar training states.

The mean squared error was utilized as the loss function, and it included a term regarding the standard deviation on the test error. This allowed to account for the set of hyperparameters that yields the low uncertainty on the model's final state, Eq. (3).

$$MSE_i = \frac{1}{K_S}\sum_{K_S=1}^{N}\left(\frac{1}{N}\sum(y-\hat{y})^2\right)+\sigma_i \tag{3}$$

Where K_S was the number of shuffle iterations, $\hat{y}$ was the vector of experimental values corresponding to the pollutant's concentration and y was the vector for the model predictions. According to this, the standard deviation σ_i was computed based on a total of 10 random shuffles.

2.3.1. Neural network

A two-hidden layers (HL) feed-forward neural network was employed based on previous architectures reporting satisfactory results predicting AOPs kinetics (Mojiri et al., 2019; Rayssa et al., 2020; Nasseh et al., 2022). A rectifier linear unit (ReLU) was added after each HL to introduce nonlinearity, Eq. (4). This activation function is known to require less computational resources than hyperbolic tangent and sigmoid activations (Dubey et al., 2022) and has been previously applied in studies involving chemical processes (Gbadago et al., 2021; Murakami and Shono, 2022).

$$f(x) = \begin{cases} x & x > 0 \\ 0 & x \leq 0 \end{cases} \tag{4}$$

Training was carried up to 80 epochs through the adaptive moment optimizer (Adam) which combined features from the AdaGrad (Duchi et al., 2011) and RMSProp optimizers (Tieleman and Hinton, 2012). This method has been widely implemented with satisfactory results (Ruder, 2016; Hassan et al., 2022). The generalized network architecture is depicted in Fig. 3.

The learning rate was set to 0.001, according to the default value provided in the work from Khingma and Lei (Kingma and Ba, 2014). Also, a grid search from 1 to 20 training batches and 15–500 neurons per hidden layer was evaluated to find the best training configuration.

2.3.2. Support vector regression

The theory and fundamentals on support vector machine (SVM) were first developed by Vapnik et al. (Vapnik, 1963; Vapnik, 1998). Since then, SVM has become a powerful machine learning technique with applications in classification and regression problems (Pandit and Kolios, 2020; Ting et al., 2020; Nasir et al., 2022). In the case of support Vector Regression (SVR), the ε parameter is employed as a threshold coefficient to deal with overfitting issues. The primal representation for a non-linear SVR problem is presented in Eqs. (4) - (5).

$$\min \frac{1}{2}\|w\|^2 + C\sum_{i=1}^{N}\left(\xi_i+\xi_i^*\right) \tag{4}$$

Subject to

$$\begin{aligned} y_i - w^T\varphi(x_i) &\leq \varepsilon+\xi_i^* \quad i=1,\ldots,N \\ w^T\varphi(x_i) - y_i &\leq \varepsilon+\xi_i \quad i=1,\ldots,N \\ \xi_i,\xi_i^* &\geq 0 \quad i=1,\ldots,N \end{aligned} \tag{5}$$

Where $\varphi(x_i)$ represents the non-linear transformation of the input features to the kernel space. From Eq. (4) it can be seen from the terms on the right side that they are indicators for the function flatness and prediction error, according to the first and second terms, respectively. As such, the trade-off parameter C establishes the importance towards the prediction error for a given regression problem.

Additional information regarding the mathematical treatments to solve this optimization problem can be consulted in (Smola and Schölkopf, 2004). This work implemented the radial basis function (RBF) as the non-linear kernel (Salcedo-Sanz et al., 2014) for the SVR model and a grid search was implemented for values of C and γ ranging from 1 to 2000, and 0.1 - 2.0, respectively. Meanwhile, the parameter was manually set to a fixed value ε_k.

2.4. Sensitivity analysis

After evaluating the models' performance, a global sensitivity analysis method was implemented to assess the effect of variance in the input variables over the model response. These techniques provide important advantages over the local sensitivity analysis methods as they allow the exploration of large variations and can also quantify uncertainty in the

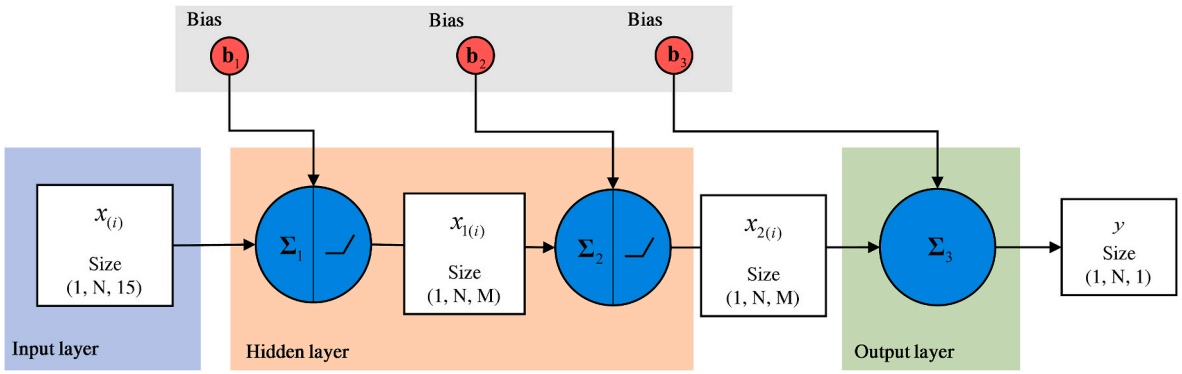

Fig. 4. ANN architecture for an arbitrary configuration with M neurons per HL and input size N.

model output regarding the variance in the inputs. Such an advantage brings a more complete characterization of the input's contributions, which is especially valuable for non-linear models (Kramer et al., 1984).

In the present study, the Fourier Amplitude Sensitivity Test (FAST) was implemented. Its main idea consists of assigning a signal to each of the model's parameters by generating periodic samples, then, a Fourier transformation is applied to decompose variance in the output into partial variance due to the parameters (Xu and Gertner, 2011). This work does not delve into the mathematical treatment for this method since it lies out of the scope of the present study. The complete mathematical treatment of the FAST method can be consulted in the works of Cukier et al., 1973, 1975, 1978.

2.5. Cost estimation

The AOPs implementation costs were estimated in terms of the sum for electrical power and reagent consumption. The price information is provided in Table 5. Since the Ti-Nw catalyst was synthesized at laboratory scale, no price information was available. Therefore, it was considered the same as the Ti-p25 (see Table 6).

The electrical power consumption was estimated based in the expenses for the UV lamps, ozonator, and rotor, according to Eq. (7), where P_{Lamps} had a fixed value of 0.04 kWh, and ζ was a piecewise function given by Eq. (8). The rotor consumption was computed as a linear function of the stirring speed using the maximum stirring speed and power consumption as reference values, as shown in Eq. (9), and the electrical consumption for the ozone production was computed according to Fig. S1 for the corresponding resistor level for the desired ozone concentration.

$$\varphi_P = \chi_E t\left(P_{Rotor} + P_{O_3} + \zeta P_{Lamps}\right) \tag{7}$$

$$\zeta = \begin{cases} 1, & \text{UV} \\ 0, & \text{No UV} \end{cases} \tag{8}$$

$$P_{Rotor} = P_{Rotor}^{Max}\frac{\omega_{rpm}}{\omega_{rpm}^{Max}} \tag{9}$$

Regarding the consumptions of reagents, the costs for hydrogen peroxide was calculated according to Eq. (10), where $\rho_{H_2O_2}$ was the commercial solution (30% w/w H_2O_2), $\rho^*_{H_2O_2}$ was the corresponding density after dilution in the system, and V was the volume of liquid within the reactor.

$$\varphi_{H_2O_2} = \chi_{H_2O_2}\frac{\rho^*_{H_2O_2}V}{\rho_{H_2O_2}} \tag{10}$$

For the case of oxygen consumption, its cost was simply computed in terms of the gas flow rate Q_G, as shown in Eq. (11).

$$\varphi_{O_2} = \chi_{O_2} Q_G t \tag{11}$$

Finally, the cost for catalyst consumption was computed from Eq. (12) as a function of the catalyst load C_{mp}. It was considered that each catalyst batch could be utilized three times before losing activity, such an assumption was made to approximate real conditions where catalysts are expected to be reutilized several times.

$$\varphi_{Cat} = \frac{1}{3}\chi_{cat} C_{mp} V \tag{12}$$

Table 5
Unit costs for reagents, catalysts, and electrical power.

Resources	Variable	Cost	Units	References
Electrical power	χ_E	0.19	$\$\, kW^{-1}h^{-1}$	(EMCALI Tarifas de Energía)
Oxygen	χ_{O_2}	1.09	$\$\, L^{-1}$	(Air-Products Industrial Oxygen Gas Cylinders)
Hydrogen Peroxide	$\chi_{H_2O_2}$	16.81	$\$\, L^{-1}$	(Spectrum-Chemical Hydrogen Peroxide Solution 30)
TiO_2[a], [b]	χ_{Cat}	0.66	$\$\, g^{-1}$	(FisherScientific Titanium)
FeOOH		0.63		(Sigmaaldrich)

[a] Aeroxide p-25.
[b] Titania nano-wires.

Table 6
Boundaries for the multi-objective optimization problem.

Variables	Min. value	Max. value	Units
ϖ_{O_3}	0.0	100.0	%
$\hat{c}_{H_2O_2}$	0.0	16.0	ppm
Q_G	0.0	3.0	$L\ min^{-1}$
ω	900.0	1500.0	rpm
I_0	0.0	1.0	
C_{mp}	0.0	1.0	$g\ L^{-1}$

2.6. Multi-objective optimization

The NSGA-II (Deb et al., 2002) algorithm was implemented to find the set of non-dominated solutions that maximized degradation and minimized costs. The inputs for the initial PhACs concentration and reaction volume were kept constant with values of 0.101 mM and 4.5 L, respectively, for a reaction period of 10 min. The optimization variables were listed in Table 7.

The objective functions are presented in Eqs. (13) and (14). Where the function f was the selected machine learning model to predict the PhACs removal and X was the corresponding input vector. Meanwhile, Eq. (14) represented the sum of the costs associated to the electrical consumption φ_E, reagents consumption φ_{O_2}, and $\varphi_{H_2O_2}$, and catalyst consumption φ_{Cat}.

$$\min\ f(X) \tag{13}$$

$$\min \sum \varphi_i \tag{14}$$

The analysis was performed independently evaluating the degradation performance for each catalyst over the different PhACs. Since the volume, catalyst and molecular properties were known as they were kept constant, the descriptors x^*_2, x^*_6, x^*_7, x^*_8, x^*_9, x^*_{10}, x^*_{13}, and x^*_{14} were not changed during independent optimizations. Meanwhile, x^*_3 was computed based on ϖ_{O_3} and Q_G, interpolating through Fig. S1a. Then, after estimating the ozone concentration, the feature x^*_5 was determined

Table 7
Mean values for the models' relative errors per process and number of samples N.

Process	Models	IBP		DCF		CAF	
		Error (%)	N	Error (%)	N	Error (%)	N
O_3	ANN	15.1	20	14.7	52	18.9	44
	SVR	42.8		21.5		15.7	
O_3/Catalyst	ANN	20.0	12	15.5	125	9.6	69
	SVR	38.2		19.3		9.8	
O_3/Catalyst/UV	ANN	–	0	8.0	48	13.7	8
	SVR	–		22.3		11.1	
O_3/Fenton	ANN	5.6	4	–	0	–	0
	SVR	26.1		–		–	
O_3/H_2O_2	ANN	9.5	4	–	0	–	0
	SVR	31.5		–		–	
Fenton	ANN	25.4	4	–	0	–	0
	SVR	36.4		–		–	
H_2O_2	ANN	19.5	8	–	0	–	0
	SVR	114.4		–		–	
Catalyst/UV	ANN	5.1	4	20.1	24	22.3	8
	SVR	122.0		45.1		51.2	
UV	ANN	15.3	4	–	0	–	0
	SVR	162.0		–		–	

as the product between c_{O_3} and Q_G. The feature x_4^*, corresponding to hydrogen peroxide concentration was obtained converting $\widehat{c}_{H_2O_2}$ to *mM* units according to the corresponding molecular weight.

3. Results and discussion

3.1. Neural network training

The mean squared error surface (MSE) concerning the test dataset was presented in Fig. 5 based on the grid search regarding the number of training batches and neurons per HL. Large values for both variables allowed to reduce the prediction error. For the case of neurons, the error improvement was associated with the increase of parameters in the model since they enhance the ability to describe complex relations (Gad, 2018).

Despite the large number of neurons compared to the size of the training dataset, no overfitting was evidenced in Fig. 5a–b. Instead, a plateau region was achieved for the error at the test dataset using both MinMax and Z-score normalization approaches. This behavior was explained by the conservative number of training epochs that did not allow preferentially fitting the data at the cost of losing generalization (Perin Guilhermeand Buhan et al., 2021). Also, it could be seen from the error uncertainty (black dots) that the final estate of the models had good reliability. An architecture of 350 neurons per HL was selected for the final model and it was trained using 15 batches.

The model performance using MinMax and Z-score normalization approaches was presented in Fig. 6. As observed from Fig. 6a convergence was achieved for both approaches. However, the MinMax reached a narrower distance between the training and test errors compared to the Z-score results. This was associated to the strength of outlier points in the Z-score, as this regularization not only depends linearly on the mean, but also it is divided by the standard deviation. Therefore, the effect of data outliers can introduce considerable modifications in the data distribution. Meanwhile, MinMax normalization just introduced a re-scaling transformation of data from 0 to 1 (Singh and Singh, 2020; Henderi et al., 2021).

However, Fig. 6b showed that in general terms a slightly better performance was achieved through Z-score. Therefore, it was stated that selecting either of the normalization approaches will not significantly modify the final fraction of explained variance by the model. On other hand, it was observed from Fig. 6c that the model prediction error was not constant over the output domain. Instead, the observed variance declined as the PhACs concentration approached zero. It showed that the model tried to describe the dynamic nature of chemical reactions. In that sense, a phenomenological explanation would be supported on the chemical equilibrium. Hence, for an initial time t_i where the chemical potentials of reagents are high, interactions between substances should be strong (Atkins et al., 2018). But then, after a considerably long period t_∞, the chemical potentials will decay and the observed variation in the system will be negligible.

3.2. Support vector regression training

In the context of SVR training, a different behavior was observed compared to results from section 3.1. For a fixed value of $\varepsilon_k = 0.1$ a high uncertainty over the test error was observed as depicted in Fig. 7, A slight error increase was presented after C>1000, as shown in Fig. 7a–b. This was attributed to overfitting of the training dataset which reduced the model generalization capacity. It emphasized the importance of selecting proper hyperparameter values, as they strongly influence the model performance (Shekar and Dagnew, 2019; Radzi et al., 2021).

A parameters fine search within the region given by $0 < C \leq 1000$ and $0.5 \leq \gamma \leq 1.8$ through a genetic algorithm yield the hyperparameters presented in Table S1. It was observed that training through either of the normalization functions achieved similar performance, Fig. 8. The SVR models achieved similar degree of explained variance from $c_{PhACs}(t)$, but their residual distribution was more uniform compared to the observed in ANN results. This might indicate that SVR was not able to learn the dynamic behavior of variance in the output.

As observed in Fig. 8b the variance decay for low PhACs concentrations was not as evident as in Fig. 6c. This suggested that SVR was not suited to predict degradation below fixed threshold value ε_k. However, further exploration over the relative error was required to properly assess the accuracy of models. This analysis was presented is section 3.3.

3.3. Performance benchmark

No significant difference on the models' performance was appreciated by normalizing the targets through MinMax or Z-score. However, the MinMax normalization was selected to assess the models' accuracy as this would only rescale the variance in the response variable without modifying it (Singh and Singh, 2020; Henderi et al., 2021). The mean relative error was discriminated by processes and pollutants for the SVR and ANN models to compare their degree of accuracy, this information is summarized in Table 7.

It was observed that the ANN model outperformed SVR, especially in processes where data availability was limited. However, predictions were still within a large degree of uncertainty, with a maximum relative error of 25.4% for the Fenton processes. In the case of SVR larger error values were observed for most processes and the photolysis, photocatalysis, and peroxidation processes were above 100%. This demonstrated that the ε insensitivity parameter from SVR might not be a

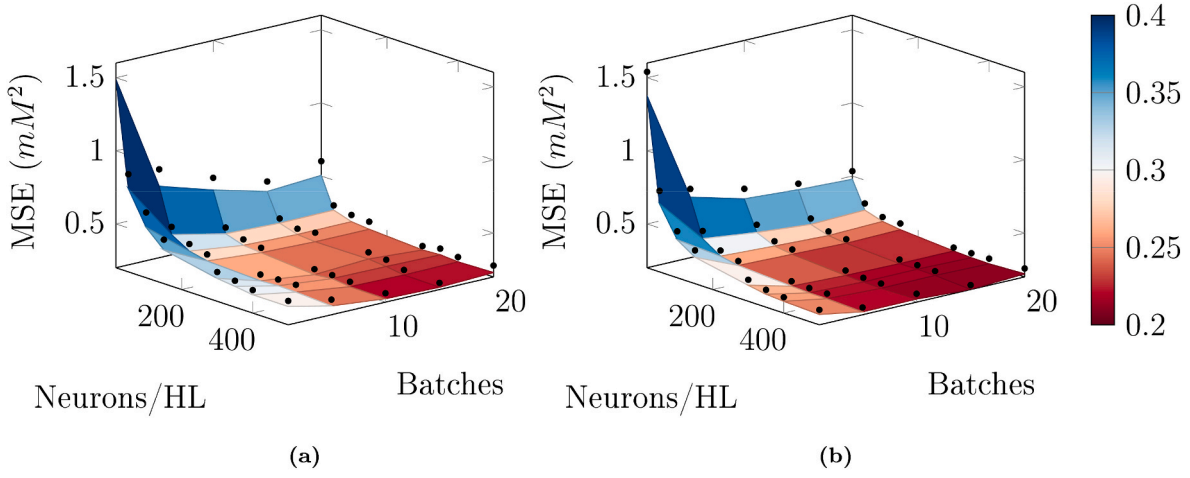

Fig. 5. Mean squared error surface for neural networks with (a) MinMax, and (b) Z-score normalizations respect to the test dataset.

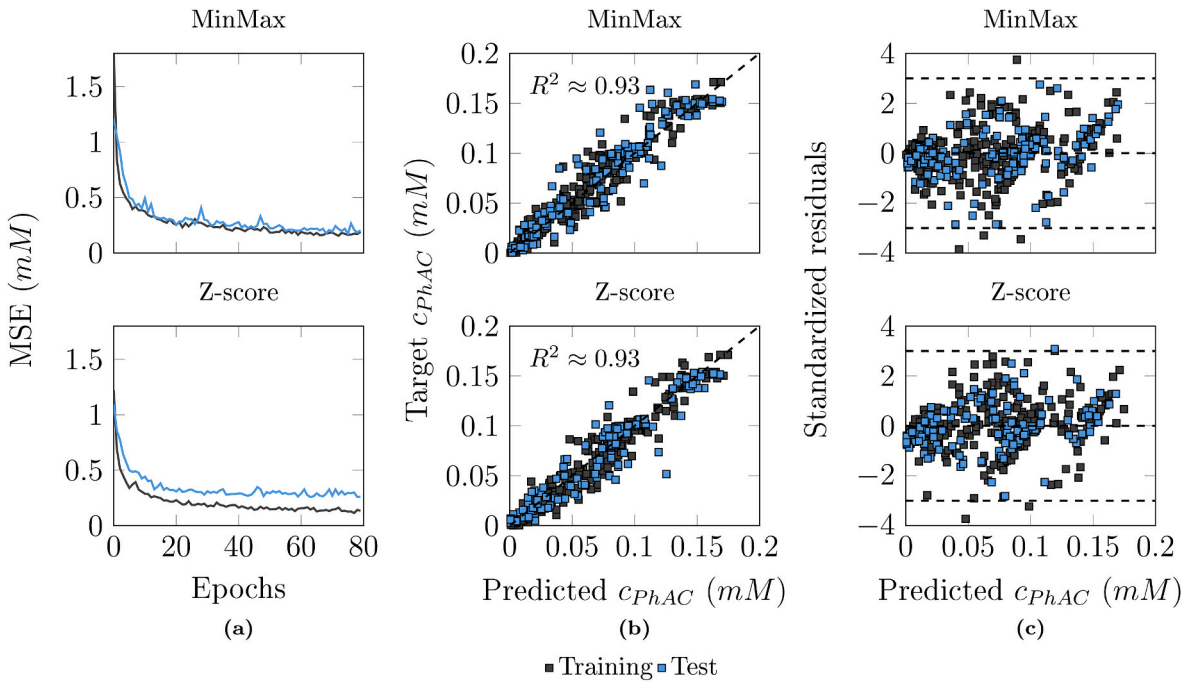

Fig. 6. MinMax and Z-score results for neural network training regarding: MSE evolution through epochs (a), predictive performance (b), and standardized residuals (c).

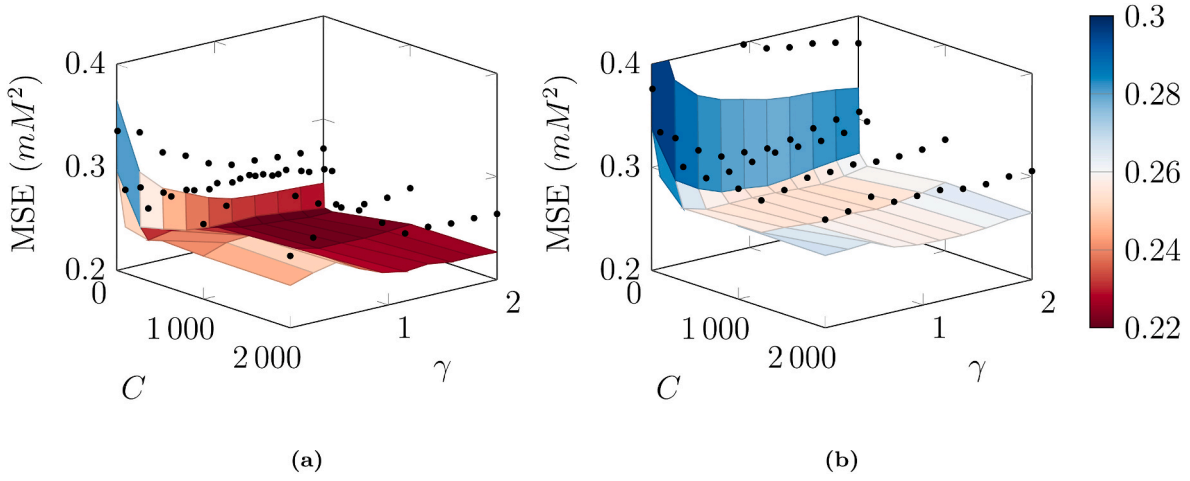

Fig. 7. Means squared error surface for SVR with (a) MinMax, and (b) Z-score normalizations respect to the test dataset.

suitable approach to predict PhACs degradation since concentrations can decay several orders of magnitude before reaching equilibria. Thus, a large error could be observed without violating the ε threshold. Predicting logarithmic concentrations or using the mean relative error as the loss function could be better alternatives to cope with this limitation.

The sensitivity analysis for the input features showed that most of the variables in the ANN model were not contributing a significant effect over the output. According to Fig. 9, the reaction time, initial concentration of pollutant, ozone concentration and mole flow were the main responsible for the variance in the output. Meanwhile, in the SVR model all the features described a significant contribution to the output. This behavior for the inputs in the SVR model was produced by the flatness term in Eq. (4). As such, the prediction error was not the only objective to minimize, but also the norm of the weights vector. Then, as the SVR can avoid assigning too large weights to control overfitting, it could also constrain the total effect assigned to a single input feature.

The large sensitivities for ozone variables in the ANN model can be explained on the fast degradation kinetic of ozone processes, as could be observed on the works from Lara et al. (Lara-Ramos et al., 2019; Lara-ram et al., 2021; Afreen et al., 2021; Lara-Ramos et al., 2021a; Lara-ramos et al., 2021). Despite the low individual values for total sensitivities in the inputs concerning to peroxide, molecular, design, and catalytic information, their sum was about 0.21, so the collective contribution could be significant. However, it was likely that the effects for I_0 and ΔE_{gap} were negligible since they presented particularly low values, about 0.01 and 0.0085. This suggested that the model neglected the effect of photolysis and photocatalysis, which could be associated to the slow kinetic regimes observed in the training data (Lara-Ramos et al., 2019).

3.4. Cost-efficiency analysis

The ANN model was utilized for the cost-efficiency analysis for degradation over 10 min, it was observed that the costs increased

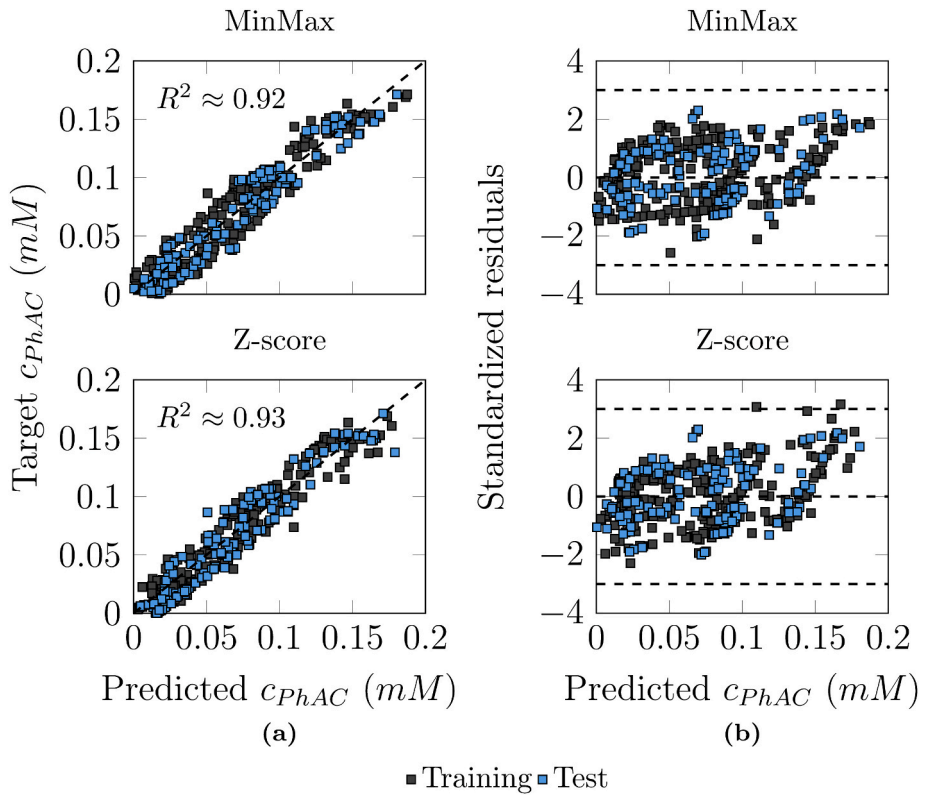

Fig. 8. MinMax and Z-score for SVR regarding predictive performance (a), and standardized residuals (b).

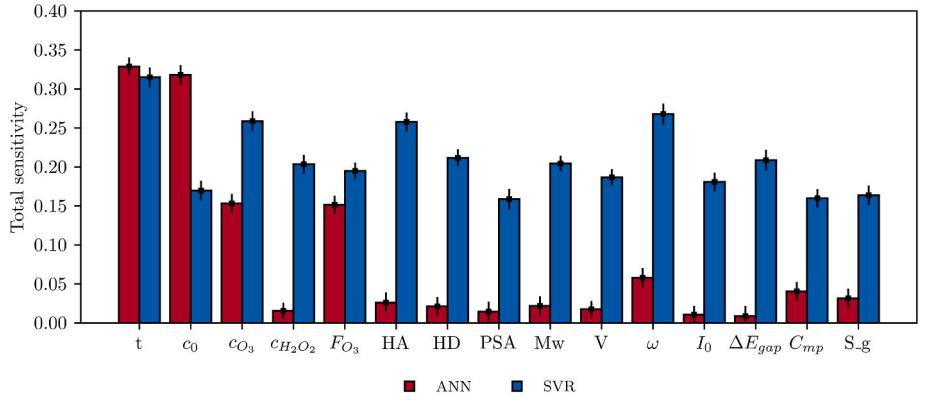

Fig. 9. Sensitivity analysis for the input features in the ANN and SVR models.

exponentially as the desired degradation approached its maximum, it is worth noting that the expected degradation values are rough estimates, therefore, this analysis rather focuses in exploring the trend for the implemented processes to maximize degradation over the different PhACs. According to the pareto front results in Fig. 10, IBP required the highest costs to reach degradations above 80%.

From the operational conditions corresponding to the set of non-dominated solutions, the use of ozone was the required to reach degradations above 50% and the FeOOH was the only catalyst within the feasible solutions, corresponding to Fenton and Fenton processes intensified with ozone. In the case of IBP degradation, the ozone-intensified Fenton was the responsible to maximize degradation up to 85%, but it also required the highest cost due to the consumption of oxygen to produce ozone through a gas flow of 2 L min^{-1}, stirring speed of 1500, 1 g L^{-1} FeOOH, and 8 ppm H_2O_2.

These results agreed with previous work since IBP rate constant for direct reaction with ozone molecule is 9.6 $M^{-1}s^{-1}$, while its coefficient for hydroxyl radicals is 7.2 $\times$ 10^9 $M^{-1}s^{-1}$ (Huber et al., 2003). Furthermore it is known that interactions between ozone molecules and carboxylic groups are not likely (Zhong et al., 2017). Meanwhile in the O_3/H_2O_2/FeOOH system, hydrogen peroxide and Fenton reactions could have contributed to decompose part of the ozone into radical species, especially, hydroxyl radicals (Beltran, 2003; Rekhate and Srivastava, 2020).

For the DCF degradation, the model suggested that a similar amount of degradation could be achieved at a lower cost through the O_3/H_2O_2 process, requiring the same conditions for IBP, but without the presence of a catalyst. According to Sein et al. (2008), during the ozone's direct attack of DCF a pathway for additional production of $HO^{\bullet}$ is triggered by the interactions with the ozone molecule and the amine group in DCF. In their study they found that diclofenac could be completely transformed with only the ozone direct attack, but also, degradation could be enhanced due to hydroxyl radicals' contribution. Although there is some discrepancy in the DCF rate constant with ozone, relatively large values

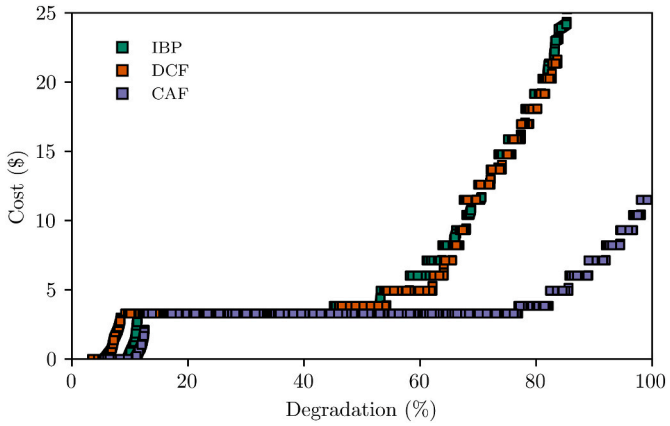

Fig. 10. Set of non-dominated solutions from the multi-objective optimization for IBP, DCF, and CAF.

have been reported, from 1.8×10^4 (Vogna et al., 2004), to $\sim 10^6$ $M^{-1}s^{-1}$ (Huber et al., 2003). Meanwhile, the corresponding DCF rate constant for interactions with $HO^{\bullet}$ has been reported as 9.29×10^9 $M^{-1}s^{-1}$ (Yang et al., 2022), which is also higher than the value for IBP.

On the other hand, this analysis suggested that caffeine described the cheapest degradation. According to the pareto front it was expected to maximize its degradation through O_3/H_2O_2 under 1 L min^{-1} gas flow and 8 ppm H_2O_2. However, this contrasted with the expected behavior as the reported rate constants for interactions with ozone were ranging between 0.82 (Rosal et al., 2009) to 673 $M^{-1}s^{-1}$ (Rosal et al., 2009), and the interactions with hydroxyl radicals were given by a rate constant of $\sim 5.9\times 10^9$ $M^{-1}s^{-1}$. These values suggested that at least a slower degradation than DCF had to be observed due to the large difference between their second order rate constants, and this was also experimentally supported by (Afreen et al., 2021).

This demonstrated that the model failed to compare kinetics between different PhACs, which might be supported by the low sensitivity indices in the molecular features, Fig. 10. Therefore, further improvement was required to implement the model as a reliable benchmarking tool. Nevertheless, despite the models' simplicity, the ANN was able to properly describe important characteristic behaviors from AOPs. Thus, it could be implemented for AOPs selection over specific pollutants to assess kinetic regimes.

4. Conclusions

The current work presented a practical ML approach to benchmark the AOPs performance for the degradation of PhACs. It was observed that the amount of explained variance was not significantly affected by the implementation of the MinMax and Z-score normalizations in the target variable, and although the SVR offered overfitting control through the ε insensitivity hyperparameter, it failed to provide good training as the threshold was not able to distinguish error at low PhACs concentrations, even for relative error values above 100%.

The cross-validation analysis showed that SVR presented limited training reliability while the ANN model was superior. According to the sensitivity analysis, the SVR could have been constrained by the ε parameter while more importance was given to the model flatness. This was supported on its even distribution over the total sensitivity coefficients, suggesting that there should not be a large distance between each of the components from the weights vector.

In contrast, for the ANN model, a large influence was observed for the time and initial concentration of PhACs, as could be expected in degradation processes. Then, followed by these features, the ozone inputs described the largest sensitivities while the remaining variables were expected to contribute through collective effects. Even so, no significant contribution was expected from UV-related inputs because the sensitivity coefficients were significantly low.

Despite the accuracy limitations in the ANN model, it could yield reasonable predictions on the behavior of different AOPs and the results were supported in literature. However, it failed to fairly compare the costs for the degradation over different PhACs, and despite the optimization analysis showed the leading role of ozone-based processes, further studies should be focused in evaluating the mineralization of the organic components as this can allow to delve on the effect of the different catalysts for the removal of degradation subproducts.

CRediT authorship contribution statement

B. Acosta-Angulo: Conceptualization, Data curation, Supervision. **J. Lara-Ramos:** Conceptualization, Methodology, Supervision. **A. Niño-Vargas:** Conceptualization, Formal analysis, Investigation. **J. Diaz-Angulo:** Conceptualization, Investigation, Supervision. **J. Benavides-Guerrero:** Conceptualization, Formal analysis, Supervision. **A. Bhattacharya:** Data curation, Investigation, Methodology, Validation, Writing – original draft. **S. Cloutier:** Conceptualization, Supervision. **F. Machuca-Martínez:** Conceptualization, Investigation, Methodology, Supervision.

Declaration of competing interest

The authors declare that they have no known competing financial interests or personal relationships that could have appeared to influence the work reported in this paper.

Data availability

Data will be made available on request.

Acknowledgements

The authors gratefully acknowledge MINCIENCIAS COLOMBIA (before known as COLCIENCIAS) for funding through the program PROCEC-AGUA contract number 80740-173-2021 with code 111585269594.

Appendix A. Supplementary data

Supplementary data to this article can be found online at https://doi.org/10.1016/j.chemosphere.2024.142222.

References

Acosta-Angulo, B., Lara-Ramos, J., Diaz-Angulo, J., Mueses, M.A., Machuca-Martínez, F., 2021. Mechanistic model and optimization of the diclofenac degradation kinetic for ozonation processes intensification. Water 13 (13), 1670. https://doi.org/10.3390/W13121670. Page 1670 2021.

Acosta-Herazo, R., Valadés-Pelayo, P.J., Mueses, M.A., Pinzón-Cárdenas, M.H., Arancibia-Bulnes, C., Machuca-Martínez, F., 2020. An optical and energy absorption analysis of the solar compound parabolic collector photoreactor (CPCP): the impact of the radiation distribution on its optimization. Chem. Eng. J. 395, 125065 https://doi.org/10.1016/J.CEJ.2020.125065.

Adam, Paszke, Sam, Gross, Francisco, Massa, Adam, Lerer, James, Bradbury, Gregory, Chanan, Trevor, Killeen, Lin, Zeming, Natalia, Gimelshein, Luca, Antiga, Alban, Desmaison, Andreas, Köpf, Yang, Edward, Zach, DeVito, Martin, Raison, Alykhan, Tejani, Sasank, Chilamkurthy, PyTorch, C.S., 2019. An Imperative Style, High-Performance Deep Learning Library.

Afreen, G., Lara-Ramos, J.A., Vidwans, N.A., Atla, V., Kumar, V., Vaddiraju, S., Machuca-Martinez, F., Sunkara, M.K., Upadhyayula, S., 2021. Bulk production of porous TiO2 nanowires by unique solvo-plasma oxidation approach for combating biotic and abiotic water contaminants. J. Mater. Sci. Mater. Electron. 32, 21974–21987. https://doi.org/10.1007/S10854-021-06642-7.

Air-products industrial oxygen gas cylinders. Available online: https://www.shopairproducts.co.uk/gases.php?gas_base=Oxygen. (Accessed 14 April 2023).

Atkins, P.W., De Paula, J., Keeler, J., 2018. Atkins' Physical Chemistry. Oxford University Press, 9780198769866.

Babuponnusami, A., Muthukumar, K., 2014. A review on Fenton and improvements to the Fenton process for wastewater treatment. J. Environ. Chem. Eng. 2, 557–572. https://doi.org/10.1016/J.JECE.2013.10.011.

Beltran, F.J., 2003. Ozone Reaction Kinetics for Water and Wastewater Systems, 9781135463076.
Ben Chabchoubi, I., Lam, S.S., Pane, S.E., Ksibi, M., Guerriero, G., Hentati, O., 2023. Hazard and health risk assessment of exposure to pharmaceutical active compounds via toxicological evaluation by zebrafish. Environ. Pollut. 324, 120698 https://doi.org/10.1016/J.ENVPOL.2022.120698.
Cherian Joel Mathewand Kumar, R., 2023. Fundamentals of machine learning. In: A Guide to Applied Machine Learning for Biologists. Springer International Publishing, Cham, pp. 147–174, 978-3-031-22206-1.
Choi, H., Baek, K., Toenjes, S.T., Gustafson, J.L., Smith, D.K., 2020. Redox-responsive H-bonding: amplifying the effect of electron transfer using proton-coupled electron transfer. J. Am. Chem. Soc. 142, 17271–17276, 10.1021/JACS.0C07841/SUPPL_FILE/JA0C07841_SI_001.PDF.
Christou, A., Karaolia, P., Hapeshi, E., Michael, C., Fatta-Kassinos, D., 2017. Long-term wastewater irrigation of vegetables in real agricultural systems: concentration of pharmaceuticals in soil, uptake and bioaccumulation in tomato fruits and human health risk assessment. Water Res. 109, 24–34. https://doi.org/10.1016/J.WATRES.2016.11.033.
Coimbra, J.T.S., Feghali, R., Ribeiro, R.P., Ramos, M.J., Fernandes, P.A., 2020. The importance of intramolecular hydrogen bonds on the translocation of the small drug piracetam through a lipid bilayer. RSC Adv. 11, 899–908. https://doi.org/10.1039/D0RA09995C.
Constantino, D.S.M., Dias, M.M., Silva, A.M.T., Faria, J.L., Silva, C.G., 2022. Intensification strategies for improving the performance of photocatalytic processes: a review. J. Clean. Prod. 340 https://doi.org/10.1016/J.JCLEPRO.2022.130800.
Cukier, R.I., Fortuin, C.M., Shuler, K.E., Petschek, A.G., Schaibly, J.H., 1973. Study of the sensitivity of coupled reaction systems to uncertainties in rate coefficients. I Theory. J. Chem. Phys. 59, 3873–3878. https://doi.org/10.1063/1.1680571.
Cukier, R.I., Schaibly, J.H., Shuler, K.E., 1975. Study of the sensitivity of coupled reaction systems to uncertainties in rate coefficients. III. Analysis of the approximations. J. Chem. Phys. 63, 1140–1149. https://doi.org/10.1063/1.431440.
Cukier, R.I., Levine, H.B., Shuler, K.E., 1978. Nonlinear sensitivity analysis of multiparameter model systems. J. Comput. Phys. 26, 1–42. https://doi.org/10.1016/0021-9991(78)90097-9.
Deb, K., Pratap, A., Agarwal, S., Meyarivan, T., 2002. A fast and elitist multiobjective genetic algorithm: nsga-II. IEEE Trans. Evol. Comput. 6, 182–197. https://doi.org/10.1109/4235.996017.
Diaz-Angulo, J., Gomez-Bonilla, I., Jimenez-Tohapanta, C., Mueses, M., Pinzon, M., Machuca-Martinez, F., 2019. Visible-light activation of TiO2 by dye-sensitization for degradation of pharmaceutical compounds. Photochem. Photobiol. Sci. 18, 897–904. https://doi.org/10.1039/C8PP00270C.
Ding, H., Hu, J., 2021. Degradation of carbamazepine by UVA/WO3/hypochlorite process: kinetic modelling, water matrix effects, and density functional theory calculations. Environ. Res. 201, 111569 https://doi.org/10.1016/J.ENVRES.2021.111569.
Dubey, S.R., Singh, S.K., Chaudhuri, B.B., 2022. Activation functions in deep learning: a comprehensive survey benchmarkand. Neurocomputing 503, 92–108. https://doi.org/10.1016/J.NEUCOM.2022.06.111.
Duchi, J., Hazan, E., Singer, Y., 2011. Adaptive subgradient methods for online learning and stochastic optimization. J. Mach. Learn. Res. 12, 2121–2159.
EMCALI Tarifas de Energía. Mercado regulado: $/kWh. Available online: https://www.emcali.com.co/web/energia/mercado-regulado. (Accessed 15 April 2023).
Feijoo, S., Yu, X., Kamali, M., Appels, L., Dewil, R., 2023. Generation of oxidative radicals by advanced oxidation processes (AOPs) in wastewater treatment: a mechanistic, environmental and economic review. Rev. Environ. Sci. Bio/Technology 221 (22), 205–248. https://doi.org/10.1007/S11157-023-09645-4, 2023.
Fischbacher, A., Von Sonntag, J., Von Sonntag, C., Schmidt, T.C., 2013. The •oH radical yield in the H2O2 + O3 (peroxone) reaction. Environ. Sci. Technol. 47, 9959–9964. https://doi.org/10.1021/ES402305R/ASSET/IMAGES/MEDIUM/ES-2013-02305R_0005.GIF.
FisherScientific titanium(IV) oxide, Aeroxide(R) P25, thermo scientific chemicals | Fisher scientific Available online: https://www.fishersci.com/shop/products/titanium-iv-oxide-aeroxide-r-p25-thermo-scientific/AC384290010 (accessed on April 14, 2023).
Gad, A.F., 2018. Artificial neural networks. Pract. Comput. Vis. Appl. Using Deep Learn. with CNNs 45–106. https://doi.org/10.1007/978-1-4842-4167-7_2.
Gao, H., Zhu, L.-T., Luo, Z.-H., Fraga, M.A., Hsing, I.-M., 2022. Machine learning and data science in chemical engineering. Ind. Eng. Chem. Res. 61, 8357–8358. https://doi.org/10.1021/acs.iecr.2c01788.
Gbadago, D.Q., Moon, J., Kim, M., Hwang, S., 2021. A unified framework for the mathematical modelling, predictive analysis, and optimization of reaction systems using computational fluid dynamics, deep neural network and genetic algorithm: a case of butadiene synthesis. Chem. Eng. J. 409, 128163 https://doi.org/10.1016/J.CEJ.2020.128163.
Hassan, E., Shams, M.Y., Hikal, N.A., Elmougy, S., 2022. The effect of choosing optimizer algorithms to improve computer vision tasks: a comparative study. Multimed. Tools Appl. 82, 16591–16633. https://doi.org/10.1007/S11042-022-13820-0/FIGURES/23.
He, Z., Zheng, H., Zeng, G., Yang, Z., Wang, H., Qin, X., Xiang, Y., Sengupta, A., Zhao, Z., Pu, S., 2023. Structurally optimized MXene-based photocatalytic membrane to achieve self-cleaning properties and enhanced removal for small molecule from wastewater. Sep. Purif. Technol. 324, 124542 https://doi.org/10.1016/j.seppur.2023.124542.
Henderi, H., Wahyuningsih, T., Rahwanto, E., 2021. Comparison of Min-Max Normalization and Z-Score Normalization in the K-Nearest Neighbor (kNN) Algorithm to Test the Accuracy of Types of Breast Cancer.
Huang, Y., Li, T., Zheng, S., Fan, L., Su, L., Zhao, Y., Xie, H.-B., Li, C., 2020. QSAR modeling for the ozonation of diverse organic compounds in water. Sci. Total Environ. 715, 136816 https://doi.org/10.1016/j.scitotenv.2020.136816.
Huber, M.M., Canonica, S., Park, G.Y., Von Gunten, U., 2003. Oxidation of pharmaceuticals during ozonation and advanced oxidation processes. Environ. Sci. Technol. 37, 1016–1024. https://doi.org/10.1021/ES025896H.
Ji, H., Lan, Y., Nie, S., Qin, T., Nie, S., Zhou, J., 2022. Synergistic effect of hydrodynamic cavitation characteristics of self-excited oscillation cavity for degradation of dye wastewater. J. Clean. Prod. 380, 135116 https://doi.org/10.1016/J.JCLEPRO.2022.135116.
Kingma, D.P., Ba, J.L., 2014. Adam: A Method for Stochastic Optimization. 3rd Int. Conf. Learn. Represent. ICLR 2015 - Conf. Track Proc.
Kramer, M.A., Rabitz, H., Calo, J.M., Kee, R.J., 1984. Sensitivity analysis in chemical kinetics: recent developments and computational comparisons. Int. J. Chem. Kinet. 16, 559–578. https://doi.org/10.1002/KIN.550160506.
Kumar, M., Sridharan, S., Sawarkar, A.D., Shakeel, A., Anerao, P., Mannina, G., Sharma, P., Pandey, A., 2023. Current research trends on emerging contaminants pharmaceutical and personal care products (PPCPs): a comprehensive review. Sci. Total Environ. 859, 160031 https://doi.org/10.1016/J.SCITOTENV.2022.160031.
Lara-Ramos, J.A., Sánchez-Gómez, K., Valencia-Rincón, D., Diaz-Angulo, J., Mueses, M., Machuca-Martínez, F., 2019. Intensification of the O3/TiO2/UV advanced oxidation process using a modified flotation cell. Photochem. Photobiol. Sci. 18, 920–928. https://doi.org/10.1039/c8pp00308d.
Lara-Ramos, J.A., Constain-Escobar, A.M., Rojas-Ortiz, K.V., Diaz-Angulo, J., Machuca-Martínez, F., 2021a. A novel high rotation bubble reactor for the treatment of a model pollutant in ozone/goethite/H2O2 and UV/goethite coupled processes. Environ. Sci. Pollut. Res. 28, 24079–24091. https://doi.org/10.1007/S11356-020-12299-2/FIGURES/10.
Lara-Ramos, J.A., Diaz-Angulo, J., Machuca-Martínez, F., 2021b. Use of modified flotation cell as ozonation reactor to minimize mass transfer limitations. Chem. Eng. J. 405, 126978 https://doi.org/10.1016/J.CEJ.2020.126978.
Lara-ramos, J.A., Figueroa-Angulo, M.A., Machuca martínez, F., Mueses, M.A., 2021. Sensitivity analysis of the catalytic ozonation under different kinetic modeling approaches in the diclofenac degradation. Water 13, 3003. https://doi.org/10.3390/W13213003. Page 3003 2021, 13.
Li, H., Yi, F., Li, X., Gao, X., 2021. Numerical modeling of mass transfer processes coupling with reaction for the design of the ozone oxidation treatment of wastewater. Front. Chem. Sci. Eng. 15, 602–614. https://doi.org/10.1007/s11705-020-1963-4.
Lian, B., Jiang, Q., Garg, S., Wang, Y., Yuan, Y., Waite, T.D., 2022. Analysis of ozonation processes using coupled modeling of fluid dynamics, mass transfer, and chemical reaction kinetics. Environ. Sci. Technol. 56, 4377–4385. https://doi.org/10.1021/ACS.EST.1C07694.
Liu, J., Jia, H., Mei, M., Wang, T., Chen, S., Li, J., 2022. Efficient degradation of diclofenac by digestate-derived biochar catalyzed peroxymonosulfate oxidation: performance, machine learning prediction, and mechanism. Process Saf. Environ. Prot. 167, 77–88. https://doi.org/10.1016/j.psep.2022.09.007.
Majumder, A., Gupta, A.K., Ghosal, P.S., Varma, M., 2021. A review on hospital wastewater treatment: a special emphasis on occurrence and removal of pharmaceutically active compounds, resistant microorganisms, and SARS-CoV-2. J. Environ. Chem. Eng. 9, 104812 https://doi.org/10.1016/J.JECE.2020.104812.
McMurry, J., 2003. Fundamentals of Organic Chemistry. Thomson-Brooks/Cole, 9780534395735.
Méndez-Arriaga, F., Torres-Palma, R.A., Pétrier, C., Esplugas, S., Gimenez, J., Pulgarin, C., 2009. Mineralization enhancement of a recalcitrant pharmaceutical pollutant in water by advanced oxidation hybrid processes. Water Res. 43, 3984–3991. https://doi.org/10.1016/J.WATRES.2009.06.059.
Mojiri, A., Vakili, M., Farraji, H., Aziz, S.Q., 2019. Combined ozone oxidation process and adsorption methods for the removal of acetaminophen and amoxicillin from aqueous solution; kinetic and optimisation. Environ. Technol. Innov. 15, 100404 https://doi.org/10.1016/J.ETI.2019.100404.
Murakami, Y., Shono, A., 2022. Reaction engineering with recurrent neural network: kinetic study of Dushman reaction. Chem. Eng. J. Adv. 9, 100219 https://doi.org/10.1016/J.CEJA.2021.100219.
Nasir, N., Kansal, A., Alshaltone, O., Barneih, F., Sameer, M., Shanableh, A., Al-Shamma'a, A., 2022. Water quality classification using machine learning algorithms. J. Water Process Eng. 48, 102920 https://doi.org/10.1016/j.jwpe.2022.102920.
Nasseh, N., Samadi, M.T., Ghadirian, M., Hossein Panahi, A., Rezaie, A., 2022. Photocatalytic degradation of tamoxifen by using a novel synthesized magnetic nanocomposite of FeCl2@ac@ZnO: a study on the pathway, modeling, and sensitivity analysis using artificial neural network (AAN). J. Environ. Chem. Eng. 10, 107450 https://doi.org/10.1016/J.JECE.2022.107450.
Ngo, T.C., Taamalli, S., Srour, Z., Fèvre-Nollet, V., El Bakali, A., Louis, F., Černušák, I., Dao, D.Q., 2023. Theoretical insights into the oxidation of quinmerac herbicide initiated by HO• radical in aqueous media: mechanism, kinetics, and ecotoxicity. J. Environ. Chem. Eng. 11, 109941 https://doi.org/10.1016/j.jece.2023.109941.
Pandit, R., Kolios, A., 2020. SCADA data-based support vector machine wind turbine power curve uncertainty estimation and its comparative studies. Appl. Sci. 10 https://doi.org/10.3390/app10238685.
Pathapati, S.S., Mazzei, A.L., Jackson, J.R., Overbeck, P.K., Bennett, J.P., Cobar, C.M., 2016. Optimization of mixing and mass transfer in in-line multi-jet ozone contactors using computational fluid dynamics. Ozone Sci. Eng. 38, 245–252. https://doi.org/10.1080/01919512.2016.1188682.
Pedregosa Fabianpedregosa, F., Michel, V., Grisel Oliviergrisel, O., Blondel, M., Prettenhofer, P., Weiss, R., Vanderplas, J., Cournapeau, D., Pedregosa, F.,

Varoquaux, G., et al., 2011. Scikit-learn: machine learning in Python. J. Mach. Learn. Res. 12, 2825–2830. https://doi.org/10.5555/1953048.2078195.
Perin Guilhermeand Buhan, I., Learning, P.S., 2021. When to stop: a mutual information approach to prevent overfitting in profiled side-channel analysis. In: Proceedings of the Constructive Side-Channel Analysis and Secure Design. Springer International Publishing, Cham, pp. 53–81.
Prasanna, S., Doerksen, R.J., 2009. Topological polar surface area: a useful descriptor in 2D-QSAR. Curr. Med. Chem. 16, 21. https://doi.org/10.2174/092986709787002817.
Radzi, S.F.M., Karim, M.K.A., Saripan, M.I., Rahman, M.A.A., Isa, I.N.C., Ibahim, M.J., 2021. Hyperparameter tuning and pipeline optimization via grid search method and tree-based AutoML in breast cancer prediction. J. Pers. Med. 11 https://doi.org/10.3390/jpm11100978.
Rayssa, A., Feliciano, S., Andrade De Lucena, A.L., Magali Da, R., Santana, R., Mendes, E., Zaidan, C., Michelle Da Silva, P., Napoleão, H., Menezes, M.M., et al., 2020. Advanced oxidation processes employment for the degradation of lamivudine: kinetic assessment, toxicity study and mathematical modeling. Water Qual. Res. J. 55, 249–260. https://doi.org/10.2166/WQRJ.2020.010.
Rekhate, C.V., Srivastava, J.K., 2020. Recent advances in ozone-based advanced oxidation processes for treatment of wastewater- A review. Chem. Eng. J. Adv. 3 https://doi.org/10.1016/J.CEJA.2020.100031.
Rodríguez-Chueca, J., Carbajo, J., García-Muñoz, P., 2023. Intensification of photo-assisted advanced oxidation processes for water treatment: a critical review. Catal 13, 401. https://doi.org/10.3390/CATAL13020401, 2023, 13, 401.
Rosal, R., Rodríguez, A., Perdigón-Melón, J.A., Petre, A., García-Calvo, E., Gómez, M.J., Agüera, A., Fernández-Alba, A.R., 2009. Degradation of caffeine and identification of the transformation products generated by ozonation. Chemosphere 74, 825–831. https://doi.org/10.1016/J.CHEMOSPHERE.2008.10.010.
Ruder, S., 2016. An Overview of Gradient Descent Optimization Algorithms.
Salcedo-Sanz, S., Rojo-Álvarez, J.L., Martínez-Ramón, M., Camps-Valls, G., 2014. Support vector machines in engineering: an overview. WIREs Data Min. Knowl. Discov. 4, 234–267. https://doi.org/10.1002/widm.1125.
Sein, M.M., Zedda, M., Tuerk, J., Schmidt, T.C., Golloch, A., von Sonntag, C., 2008. Oxidation of diclofenac with ozone in aqueous solution. Environ. Sci. Technol. 42, 6656–6662. https://doi.org/10.1021/es8008612.
Shahsavar, F., Zahedi, E., Shiroudi, A., Chahkandi, B., 2023. Atmospheric degradation mechanism of anthracene initiated by OH•: a DFT prediction. J. Mol. Graph. Model. 121, 108426 https://doi.org/10.1016/j.jmgm.2023.108426.
Shekar, B.H., Dagnew, G., 2019. Grid search-based hyperparameter tuning and classification of microarray cancer data. In: Proceedings of the 2019 Second International Conference on Advanced Computational and Communication Paradigms (ICACCP), pp. 1–8.
Singh, D., Singh, B., 2020. Investigating the impact of data normalization on classification performance. Appl. Soft Comput. 97, 105524 https://doi.org/10.1016/j.asoc.2019.105524.
Sirés, I., Brillas, E., Oturan, M.A., Rodrigo, M.A., Panizza, M., 2014. Electrochemical advanced oxidation processes: today and tomorrow. A review. Environ. Sci. Pollut. Res. 21, 8336–8367. https://doi.org/10.1007/S11356-014-2783-1/TABLES/4.
Smith, D.K., 2021. Exploring the role of H-bonding in organic electrochemistry – from supramolecular applications to mechanistic investigations. Chem. Rec. 21, 2488–2501. https://doi.org/10.1002/TCR.202100186.
Smola, A.J., Schölkopf, B., 2004. A tutorial on support vector regression. Stat. Comput. 14, 199–222. https://doi.org/10.1023/B:STCO.0000035301.49549.88/METRICS.
Spectrum-chemical hydrogen peroxide solution 30 percent reagent ACS | H1065. Available online: https://www.spectrumchemical.com/hydrogen-peroxide-solution-30-percent-reagent-acs-h1065. (Accessed 14 April 2023).
Svebrant, S., Spörndly, R., Lindberg, R.H., Sköldstam, T.O., Larsson, J., Öhagen, P., Lindström, H.S., Järhult, J.D., 2021. On-site pilot testing of hospital wastewater ozonation to reduce pharmaceutical residues and antibiotic-resistant bacteria. Antibiotics 10, 684. https://doi.org/10.3390/ANTIBIOTICS10060684/S1.
Tangestani, E., Keivanimehr, F., Ghadiri, M., 2021. Insights into the estimation of hydroxyl radical rate constant of water contaminants in AOP using new smart QSPR models. Water Environ. J. 35, 312–321. https://doi.org/10.1111/wej.12628.
Telikani, A., Tahmassebi, A., Banzhaf, W., Gandomi, A.H., 2021. Evolutionary machine learning: a survey. ACM Comput. Surv. 54 https://doi.org/10.1145/3467477.
Tieleman, T., Hinton, G., 2012. Rmsprop: divide the gradient by a running average of its recent magnitude. Lecture 6.5.
Ting, W.-C., Chang, H.-R., Chang, C.-C., Lu, C.-J., 2020. Developing a novel machine learning-based classification scheme for predicting SPCs in colorectal cancer survivors. Appl. Sci. 10 https://doi.org/10.3390/app10041355.
Tong, K., Yang, L., Du, X., 2020. Modelling of TiO2-based packing bed photocatalytic reactor with Raschig rings for phenol degradation by coupled CFD and DEM. Chem. Eng. J. 400 https://doi.org/10.1016/J.CEJ.2020.125988.
Vapnik, V., 1963. Pattern recognition using generalized portrait method. Autom. Remote Control.
Vapnik, V., 1998. The support vector method of function estimation. In: Suykens Johan, A.K., Vandewalle, J. (Eds.), Nonlinear Modeling: Advanced Black-Box Techniques. Springer US, Boston, MA, pp. 55–85, 978-1-4615-5703-6.
Vogna, D., Marotta, R., Napolitano, A., Andreozzi, R., D'Ischia, M., 2004. Advanced oxidation of the pharmaceutical drug diclofenac with UV/H2O2 and ozone. Water Res. 38, 414–422. https://doi.org/10.1016/J.WATRES.2003.09.028.
Xiao, R., Gao, L., Wei, Z., Spinney, R., Luo, S., Wang, D., Dionysiou, D.D., Tang, C., Yang, W., 2017. Mechanistic insight into degradation of endocrine disrupting chemical by hydroxyl radical: an experimental and theoretical approach. Environ. Pollut. 231, 1446–1452. https://doi.org/10.1016/j.envpol.2017.09.006.
Xu, C., Gertner, G., 2011. Understanding and comparisons of different sampling approaches for the fourier amplitudes sensitivity test (FAST). Comput. Stat. Data Anal. 55, 184. https://doi.org/10.1016/J.CSDA.2010.06.028.
Yang, J., Lv, G., Li, T., Sun, S., Sun, X., 2022. Theoretical insight into the degradation of diclofenac by hydroxyl and sulfate radicals in aqueous-phase: mechanisms, kinetics and eco-toxicity. J. Environ. Chem. Eng. 10, 108311 https://doi.org/10.1016/J.JECE.2022.108311.
Yates, L.A., Aandahl, Z., Richards, S.A., Brook, B.W., 2023. Cross validation for model selection: a review with examples from ecology. Ecol. Monogr. 93, e1557 https://doi.org/10.1002/ecm.1557.
Zhong, X., Cui, C., Yu, S., 2017. Exploring the pathways of aromatic carboxylic acids in ozone solutions. RSC Adv. 7, 34339–34347. https://doi.org/10.1039/C7RA03039H.
Zhu, T., Li, S., Li, L., Tao, C., 2023. A new perspective on predicting the reaction rate constants of hydrated electrons for organic contaminants: exploring molecular structure characterization methods and ambient conditions. Sci. Total Environ. 904, 166316 https://doi.org/10.1016/j.scitotenv.2023.166316.
Iron(III) oxide hydrated, catalyst grade, 30-50mesh 20344-49-4. PubChem Substance ID: 24863095. CAS Number:20344-49-4. Available online: https://www.sigmaaldrich.com/CO/es/product/aldrich/371254 (accessed on April 14, 2023).